Finger-Operated Pumping Platform for Microfluidic Preparation of Nanoparticles

Ahmed Azmeer[1§‡], Ibraheem Kanan,[1‡] Ghaleb A. Husseini[2*], Mohamed Abdelgawad[1,3*]

[1] Department of Mechanical Engineering, American University of Sharjah, UAE

[2] Department of Chemical and Biological Engineering, American University of Sharjah, UAE

[3] Department of Mechanical Engineering, Assiut University, Egypt

[§] Currently with King Abdullah University of Science and Technology, Saudi Arabia

[‡] These authors contributed equally to this study.

* To whom correspondence should be addressed mabdelgawad@aus.edu, ghusseini@aus.edu

Abstract

Microfluidic preparation of nanoparticles (NPs) offers many advantages over traditional bench-top preparation techniques, including better control over particle size and higher uniformity. Although many studies have reported the use of low-cost microfluidic chips for nanoparticle synthesis, the technology is still expensive due to the high cost of the pumps needed to generate the required flows inside microchannels. Here, we present a low-cost finger-operated constant-pressure pumping platform capable of generating pressures as high as 120 kPa using finger-operated pumping caps that can be attached to any pop bottle. The platform costs around $208 and enables the generation of flow rate ratios (FRR) of up to 47:1 for the continuous flow synthesis of NPs. The pump has a resolution of 500 Pa per stroke and exhibits stable pressures for up to a few hours. To show the functionality of the proposed pump, we used it to prepare pegylated liposomes and Poly Lactic-co-glycolic acid (PLGA) nanoparticles with sizes ranging from 47 nm to 250 nm with an average polydispersity of 20% using commercially available micromixer chips and in-house made hydrodynamic flow focusing devices. We believe this platform will render microfluidic preparation of NPs accessible to any laboratory with minimal capabilities.

1 Introduction

Nanoparticles (NPs), which are particles with dimensions on the order of 100 nm or less (Khan et al. 2019), offer several advantages over traditional bulk materials, such as a high surface area to volume ratio, chemical reactivity, optical response, and biological mobility (Murthy 2007). These unique characteristics, in tandem with the surge of research on nanotechnology, resulted in the use of NPs in several areas, including drug delivery (Gujrati et al. 2014, Khan et al. 2019) (Salkho et al. 2018), medical imaging (Cheng et al. 2016), medical diagnostics (Shawky et al. 2010), photothermal therapy (Jørgensen et al. 2016), CO_2 capture technology (Ngoy et al. 2014), and nano-level energy storage applications (Liu et al. 2015).

Until recently, most NPs were synthesized using traditional “bottom-up” or “top-down” batch processes. Bottom-up methods refer to approaches based on the growth and formation of NP from smaller molecules, such as Chemical Vapor Deposition (CVD), Co-precipitation, and Sol-Gel (Adachi et al. 2003, Petcharoen and Sirivat 2012, Bokov et al. 2021). On the other hand, top-down approaches for NP synthesis rely on the breaking down of larger particles into smaller ones by applying energy into the system, such as the mechanical conversion of bulk material into nano-scale particles. Some top-down approaches for NP synthesis include thermal evaporation, laser ablation, and sputtering (Shaalan et al. 2011, Kim et al. 2017, Nguyen et al. 2017).

Despite their wide adaptation, traditional “bottom-up” and “top-down” batch techniques suffer numerous drawbacks, largely stemming from a lack of accurate control over experimental variables. As a result, there is often large inter-batch variation in synthesized NP sizes, leading to unsatisfactory performance of the NPs during application (Liu and Jiang 2017, Zhang et al. 2020). Other reported drawbacks of conventional NP synthesis techniques include high power consumption, overuse of materials, poor reproducibility, uncontrolled particle growth, contamination, and high polydispersity index values (Niculescu et al. 2021).

Continuous-flow microfluidics has emerged recently as a promising technology for NP synthesis due to its advantages over classical batch-to-batch techniques. These advantages include smaller particle size, reproducibility, better control over particle size, shorter reaction time, high throughput, and reduced chemical waste (Niculescu et al. 2021). Nevertheless, existing Microfluidic platforms for NP synthesis are often associated with expensive microfabrication techniques (Abualsayed et al. 2019) and bulky and expensive pumps.

Consequently, there has been a growing need to develop novel, simple microfluidic setups to synthesize NP. For example, a 3D-printed Microfluidic vortex focusing device was recently developed to reliably synthesize liposomes as small as 27 nm with the added advantage of size tunability (Han et al. 2022). A similar study used a 3D-printed flow-focusing chip to synthesize nanoliposomes as small as 100 nm in diameter (Chen et al. 2019). 3D printed microchannels were also used in several other studies involving the synthesis of silver nanoparticles, metallic core particles, and iron oxide nanoparticles (Bressan et al. 2020, Aşık et al. 2021, Kumar et al. 2023).

Although 3D printing reduces the cost of device fabrication, expensive pumps are still used to generate and precisely control flow rates inside microfluidic devices. A typical medium-level dual-channel syringe pump costs around \$4,000, whereas a dual-channel constant-pressure pump costs around \$6,000. This cost doubles or triples if the NPs formulation requires pumping multiple reagents simultaneously. Such a cost prohibits the accessibility of this technology for researchers in resource-poor settings. Recognizing this challenge, many researchers explored innovative ideas to replace the expensive regular pumping platform with simpler, lower-cost ones. For example, normal desktop centrifuges were used to drive liquids in 3D-printed microchannels designed to fit securely in falcon tubes for NP synthesis (Andrea Cristaldi et al. 2021). This setup was capable of preparing liposomes 80 – 300 nm in diameter. However, independent control of the flow inside each microchannel requires changing channel dimensions to change their resistances, complicating the device design.

Another example of a simple pumping setup for microfluidic applications relied on generating the desired pumping pressure by manually changing the volume of air trapped inside plastic syringes of multiple sizes (Moscovici et al. 2010). Nevertheless, the small volume of the syringes meant that the generated pressure could not be maintained for extended periods. A similar approach was employed in another study but using an inflated latex balloon connected to a syringe barrel carrying the fluid to be pumped into the device (Thurgood et al. 2018, Thurgood et al. 2019). Despite the simplicity of this balloon pump and its ease of use, the maximum pressure possible was less than 40 kPa, which reduces the range of possible flow rates, especially with high resistance channels. Using the potential energy stored in a stretched membrane to generate the desired pumping pressure was also demonstrated using an on-device PDMS (Poly-dimethylsiloxane) chamber with a thin top PDMS diaphragm that is stretched when the chamber is overfilled manually using a regular syringe (Gong et al. 2012). The elastic energy in the PDMS diaphragm is then used to pump the liquid out of the chamber gradually. However, the small size of the PDMS chamber renders this pumping technique non-practical for continuous flow reactors.

Another set of simple pumps relied on finger-operated pumping of flexible diaphragms incorporated either on-device (Kokalj et al. 2014, Li and Chui 2018, Park and Park 2019) or off-device (Sweet et al. 2020). While simple in principle, these pumps necessitate intricate design and fabrication, and they are unable to consistently maintain a uniform flow rate for substantial durations. The same drawbacks apply to a similar micropump constructed by a suction chamber created from a PDMS membrane integrated into the device (Lee et al. 2018).

To overcome the drawbacks of the simple pumping setups reported above, we present an inexpensive, easy-to-build, finger-operated microfluidic pump to prepare the NPs in laboratories with limited resources. Our NP synthesis platform consisted of two standard Pop bottles capped with commercially available hand-operated “fizz keeper” pumping caps. The Pop bottles served as pressurized reservoirs and were coupled to falcon tubes housing reagents for NP synthesis. The falcon tubes were then connected to the inlet of the microfluidic chip. We tested our pumping platform with a commercially available off-the-shelf herringbone micromixer chip and a PDMS hydrodynamic flow focusing chip. We characterized the pump performance in terms of the maximum pressure ratio and flow rate ratio it can generate. We also proved the pump's ability to synthesize liposomes with tunable size. We hope our setup facilitates the use of microfluidics in NP synthesis in all laboratories worldwide, regardless of their budgets and capabilities.

2 Materials and Methods

2.1 Materials

The DPPC (1,2-dipalmitoyl-sn-glycero-3-phosphocholine) and DSPE-PEG2000-NH_2 (1,2-distearoyl-sn-glycero-3-phosphoethanolamine-N-[amino(polyethyleneglycol)-2000]) were obtained from Avanti Polar Lipids Inc. (Alabaster, AL, USA). Cholesterol was obtained from

AlfaAesar (Ward Hill, MA, USA). Phosphate buffer saline (PBS) and ethanol were obtained from Laboratory Scientific Supplies (Ajman, UAE). PLGA (Poly Lactic-co-glycolic acid, AP154, 55=65 kDa, Lactic acid: glycolic acid= 50:50) was obtained from Akina Inc, Polyscitech (West Lafayette, IN). Negative photoresist (SU-8-2025) and its developer were purchased from Microresist Technologies GmbH (Berlin, Germany). We purchased Polydimethylsiloxane (PDMS) from Ellsworth Adhesives (East Kilbride, Scotland). Silicon wafers were acquired from UniversityWafer, Inc. (Boston, MA). The herringbone micromixer chips were products of the microfluidic ChipShop (Jena, Germany) and were purchased online from Darwin Microfluidics (Paris, France)

2.2 Finger Operated Pumping Setup

The heart of our finger-operated pump is two standard Pop bottles made from PET (polyethylene terephthalate) capped with commercially available "fizz keeper" pumping caps. The PET bottles serve as pressure reservoirs and are connected via PTFE (Polytetrafluoroethylene) tubing to falcon tubes, which house the reagents that will pass through the microchannels, figure 1. One additional hole is drilled in each bottle to connect it to a pressure sensor. The cap of each falcon tube was modified to have two PTFE tubes passing through them, one connected to the pressure reservoirs, and the other to transfer the solution being pumped to the microfluidic chip. Two valves were placed before the inlets of the microchannels to allow the user to stop the flow whenever necessary. Two TruStability Board Mount Pressure Sensors (Honeywell, Charlotte, NC) were connected to the two PET bottles using FEP (Fluorinated ethylene-propylene) tubing to enable the user to measure the pressure generated in the pop bottles. In addition, two SLF3S-0600F Liquid Flow Sensors (Sensirion, Stafa, Switzerland) with ranges up to 2 mL/min were connected after each valve to track the flow rates generated from the applied pressure. For higher flow rates, these two sensors were replaced with two SLF3S-1300F sensors, which can read flow rates up to 40 mL/min. Two Arduino Uno microcontrollers (purchased from Amazon) were used to read the pressure and flow rate values from the sensors. The entire setup can be placed in a compact, portable cardboard box measuring 40 cm × 30 cm, Figure 1-b. Connection diagrams and programs used to read the pressure and flow signals can be found in the Supplementary Material. A bill of items used in the construction of the pumping platform and their costs is also included in the Supplementary Material.

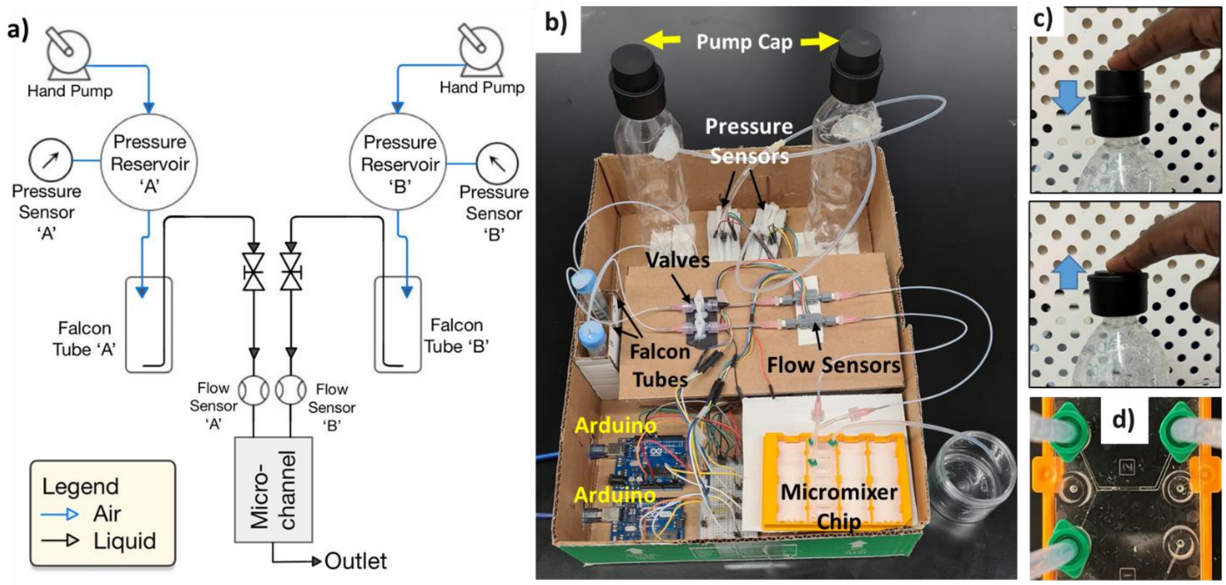

Figure 1: a) Schematic of the NP synthesis platform showing the different components of the platform and how they are connected. b) Photo of the actual pumping platform showing the two pop bottles with the pumping caps, pressure and flow sensors, and the micromixer chip. The pumping platform measures 40 cm× 30 cm. c) a close-up showing the finger-operated pump cap, d) A close-up of the herringbone micromixer chip used in liposomes preparation showing the buffer and lipid solution inlet on the left and the NP collection outlet on the right.

2.3 Pump operation

The pump operation is fairly simple. First, the falcon tubes are loaded with the solutions to be pumped, and then their caps are screwed on tightly. Then, the PET bottles are pressurized by pressing and releasing the "fizz keeper" caps multiple times (Figure 1b) until the desired pressure values are reached, as indicated by the pressure sensors for both bottles. Once the desired pressure is reached, the two valves mounted on the liquid lines are opened allowing the solutions in the falcon tubes to flow into the microfluidic chip. The generated flow rate will depend on the hydraulic resistance of the microfluidic chip and can be calculated from basic fluid mechanics relations, as explained in the theoretical section below. Alternatively, the flow sensor can be used to read the value of the generated flow rates.

2.4 Nanoparticle Synthesis

2.4.1 Preparation of Liposomes

An ethanol-based lipid solution of DPPC, cholesterol, and DSPE-PEG at concentrations of 2, 1, and 0.7 mg/mL, respectively, was loaded in one of the pump's falcon tubes, whereas PBS was loaded in the other. Then, a different number of pumping strokes was applied to each bottle to raise the pressure connected to each of the falcon tubes to the desired value as indicated by the pressure sensors. After that, the valves linking the falcon tubes to the herringbone micromixer were opened, introducing the lipid solution and PBS into separate chip inlets. The flow rate ratio (FRR) between the generated PBS and lipid solution flow rates is regulated by the pressure ratio between the pressures in the two bottles. This relationship is based on the resistances of the microchannels, as detailed in the Theoretical Analysis section below. The generated flow rates can be measured using the inline flow sensors to confirm that they agree with the theoretically calculated flow rates. Although the resulting FRR depends solely on the pressure ratio, the magnitude of the applied pressures affects the total resulting flow rate. To ensure steady operation of the system, the outlet flow from the chip in the first minute was discarded before collecting the output sample for analysis. Each FRR was tested three times. Between trials, the microchannel was flushed with methanol for ten seconds to ensure all residuals from previous trials were removed. The collected sample size from each trial was around 0.1-0.3 mL.

2.4.2 Preparation of PLGA nanoparticles

PLGA was dissolved overnight in dimethylformamide at a concentration of 5 mg/mL. The PLGA solution was loaded in one of the pump's falcon tubes, whereas DI water was loaded in the other. Then, flow generation inside the microfluidic device proceeded the same way as for the preparation of the liposomes in the above section. Two devices were used to prepare PLGA NPs, a herringbone micromixer and a hydrodynamic flow-focusing device like the one shown in Figure 2 (Abdelkarim et al. 2021). All experiments were run in triplicates.

2.4.3 Particle size measurements

The liposome size was determined by dynamic light scattering (DLS) using the DynaPro® NanoStar™ sizer (Wyatt Technology Corp., Santa Barbara, CA, USA) (Agam et al. 2024). A liposome sample of 10 μL was diluted 1:10 in PBS and loaded into a cuvette to determine the hydrodynamic radius of the prepared liposomes.

3 Theoretical Analysis

3.1 Pumping Mechanism

The setup we present here operates as a constant pressure pumping device capable of generating and maintaining the desired pressure to drive the flow. The pressure inside each of the pop bottles is governed by the ideal gas law, equation (1).

$$PV = mRT \quad (1)$$

Where P is the pressure, V is the total volume of the bottle, air portion of the falcon tube and tubing, m is the mass of the air inside this total volume, R is the gas constant, and T is the temperature of the air. Assuming that the temperature stays constant, as was confirmed through measurements, and that the total volume of the system does not change significantly, the pressure increases by ΔP with every stroke of the cap pump due to the additional mass of air Δm inserted into the bottle according to equation (2).

$$\Delta P = \frac{RT}{V} \Delta m \quad (2)$$

So, the air pressure on top of the liquid surface in the falcon tube will increase slightly with every stroke of the pump. Since the volume of the new air package inside the Fizz Keeper is constant and is always sucked from the atmosphere, its mass will be almost constant. This means that the additional mass of air introduced to the system with each stroke is constant and, therefore, the pressure increase with the number of strokes will be linear, as shown in the results section.

3.2 The theoretical relationship between Flow Rate Ratio & Pressure Ratio

Given the importance of the flow rate ratio (FRR) between the stream of the solvent and the anti-solvent in controlling the size of nanoparticles using microfluidics (Karnik et al. 2008, Michelon et al. 2017), it is desirable to control the flow rates into the microfluidic device rather than the applied pressures. The generated flow rates due to certain applied pressures can be predicted using simple fluid mechanics relations.

The FRR was defined as the ratio between the flow rate of the buffer solution (Q_1) and the lipid solution (Q_2) as outlined in equation (3) below. Similarly, the pressure ratio (PR) was defined as the ratio between the pressure of the reservoir connected to the buffer inlet (P_1) and the lipid inlet (P_2) equation (4).

$$FRR = \frac{Q_1}{Q_2} \quad (3)$$

$$PR = \frac{P_1}{P_2} \quad (4)$$

Since the flow inside the microfluidic device is laminar, the pressure drop within any microchannel is linearly proportional to the flow rate, equation (5):

$$\Delta P = R\ Q \quad (5)$$

Where R is the hydrodynamic resistance of the channel, Q is the flow rate within the channel, and ΔP is the pressure drop across the channel. The hydrodynamic resistance can be calculated using equation (6), where C is the Poiseuille number, which depends on the aspect ratio of the microchannel ($C = Reynolds\ number\ (Re) \times\ Darcyfriction\ factor\ (f)$), μ is the viscosity of the fluid, l is the length of the channel, D is the hydraulic diameter of the channel, and A is the cross-sectional area.

$$R_i = \frac{C_i \mu_i\, l_i}{2{D_i}^2 A_i} \quad (6)$$

For the case of the hydrodynamic flow focusing chip being considered here, Figure 2, equations (7) and (8) below can be used to derive a relationship between the pressure ratio and the flow ratio.

$$P_1 - P_3 = 0.5\ R_1 Q_1 + R_3 Q_3 \quad (7)$$

$$P_2 - P_3 = R_2\ Q_2 + R_3 Q_3 \quad (8)$$

The factor 0.5 is multiplied by Q_1 in equation (7) because the flow rate Q_1 is split equally into the two streams at inlet 1 and is combined again with Q_2 at the microchannel junction to create the hydrodynamic focusing effect. Also, from the conservation of mass, we have:

$$Q_3 = Q_1 + Q_2 \quad (9)$$

Re-arranging the above equations and assuming that $P_3 = 0$ since the outlet is open to the atmosphere, we arrive at equation (10) with the definitions for FRR and PR described above:

$$PR = \frac{0.5\, R_1\, FRR + R_3(1 + FRR)}{R_2 + R_3(1 + FRR)} \quad (10)$$

Re-arranging, we define the FRR as a function of PR as described by equation (11) below,

$$FRR = \frac{R_3 - PR(R_2 + R_3)}{R_3\, PR - 0.5\, R_1 - R_3} \quad (11)$$

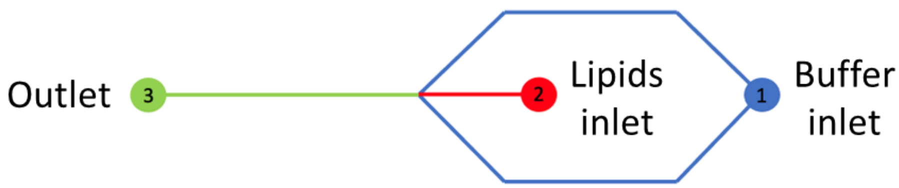

Figure 2 Schematic of the hydrodynamic flow focusing device used in the theoretical analysis of the flow rates generated using our constant pressure pumps and for preparation of the PLGA NPs by nanoprecipitation.

3.3 The use of available soft tools to predict the desired Pressure ratio

The theoretical calculations described in the previous section can be challenging for researchers with non-engineering backgrounds or if the network of channels being analyzed is more complicated. However, there are many available open-source or online tools intended to help microfluidic researchers calculate the expected flow rates/pressures inside microchannel networks or choose the proper microchannel dimension to induce a particular flow rate. Examples of these online tools are the microfluidic simulator developed by the Design Automation group at the Technical University of Munich (https://www.cda.cit.tum.de/app/mmft-simulator/) (Fink et al. 2022) and the 3DμF simulator (Sanka et al. 2019) available at (https://3duf.org/).

4 Results and Discussion

4.1 Pump Characterization

To characterize the pump capabilities, we tested the pump performance under different operating conditions. The primary goal of characterizing our pumping platform was to measure its capabilities and create accurate calibration curves to allow end users to operate it without pressure or flow sensors. As expected, the pressure increased almost linearly with the number of pumping strokes, Figure 3-a. The slight deviation from the linear relationship of equation (2) is probably because the bottle volume increases gradually at higher pressures due to strain in the bottle walls. This increase will gradually reduce the pressure rise per stroke, which agrees with the measurements.

In terms of the maximum pressure that can be generated, a pressure of 93 kPa was achieved after 30 pumping strokes with the smallest bottle volume of 325 mL (a regular pop bottle with a nominal volume of 250 mL). Higher pressures are possible with more pumping strokes, even though manual pressing of the pump cap at such high pressures becomes hard. We were able to reach pressures as high as 120 kPa with higher pressing forces.

The pump resolution, i.e., pressure rise due to one pumping stroke, was also controllable by changing the bottle volume. The larger the bottle size, the better the resolution you can achieve (i.e., smaller pressure rise). The best resolution of 500 Pa/stroke was achieved with a 2410 mL bottle, Figure 3-b. This resolution was also dependent on the existing pressure inside the pump. The higher the pressure inside the pump, the smaller the pressure rise per stroke. For example, with a bottle volume of 1335 mL, the pressure rise per stroke drops by 14% as the pressure inside the pump increases from 5 kPa to 40 kPa, Figure 3-c. This decrease is probably due to the slight increase in the bottle volume at higher pressures due to bottle expansion.

In addition, the air temperature inside the bottles was approximately constant and rose by only 3.3 °C after 30 pumping strokes, which corresponds to the highest generated pressure at a volume of 325 mL volume, Figure 1-d. In terms of pressure stability, the pressure inside the pump remained constant regardless of the number of applied strokes, Figure 3-e. The pumping cap could keep the pressure constant for a couple of hours (data not shown), which is longer than the duration of most NP synthesis experiments. If the pressure inside the pump decreases in cases of prolonged use, a few pumping strokes can be applied to bring the pressure back to its original value. The pressure sensor in the pump is a must in this case.

4.2 Controlling the flow rate ratio (FRR)

The size and polydispersity index of NPs synthesized via microfluidics are strongly dependent on the flow rate ratio between the mixing streams. Given that the current setup operates on a constant-pressure principle, the flow rate ratio is controlled by adjusting the pressure ratio (PR) between the pressure inside the two pop bottles connected to the falcon tubes. The resulting flow rate will also depend on the resistance of the microchannel in addition to the applied pressure. Predicting the FRR at a certain PR can be performed using equation (11) without adding flow sensors to the setup if the dimensions and, consequently, the hydraulic resistance of the microchannels used are known. If channel dimensions are not known, or the microchannels have irregular geometries, like the ridges of the herringbone micromixer chip used in our case, then the use of flow sensors is necessary to produce calibration curves of FRR vs. PR. Subsequently, these calibration curves enable the adjustment of the resulting FRR from knowledge of the PR only without the need for flow sensors.

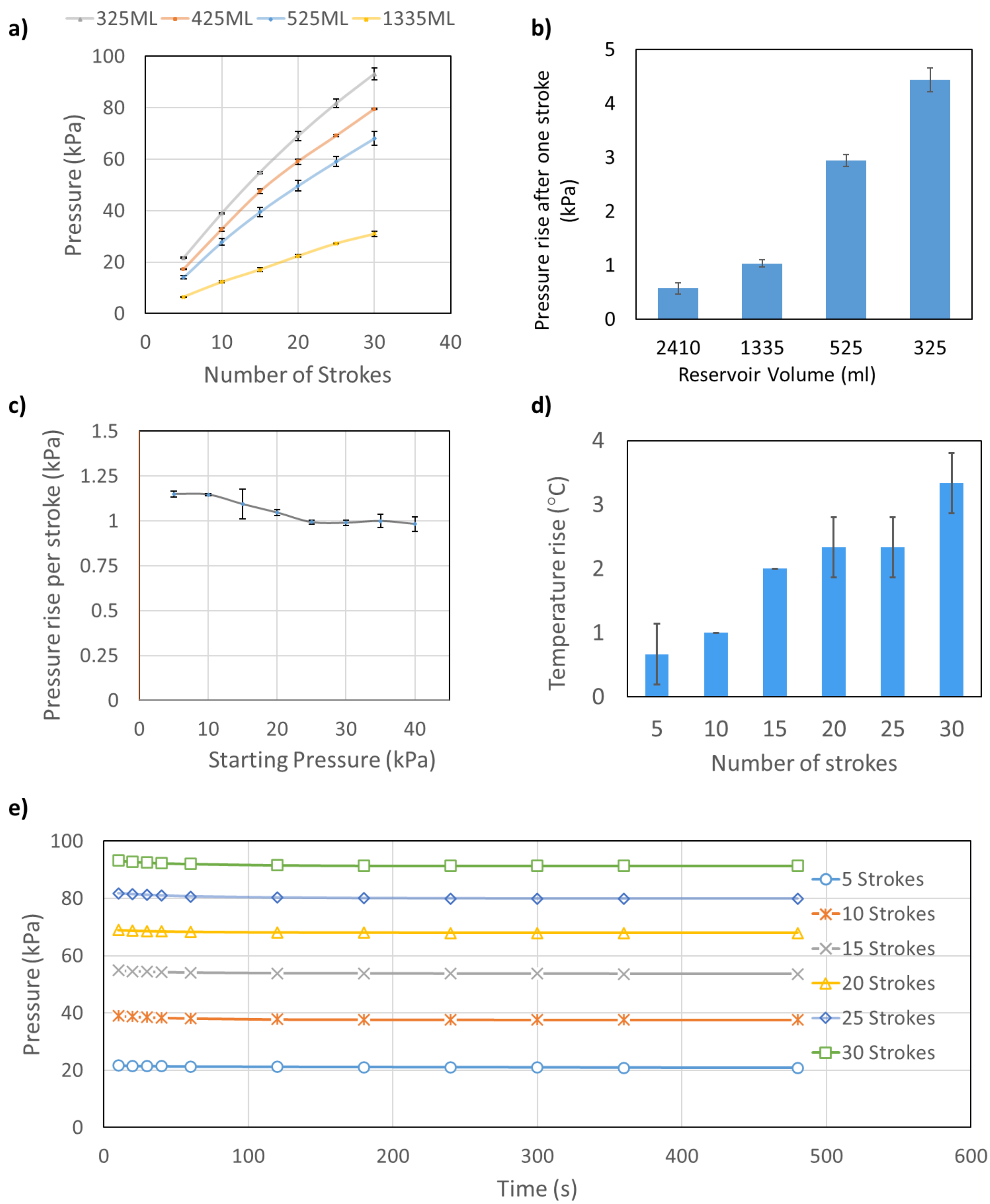

Figure 3: Characterization of the finger-operated Fizz-keeper pump. a) The generated pressure increased almost linearly with the number of pumping strokes. b) Pressure rise due to one pumping stroke at different reservoir (bottle) volumes. Using larger bottles, a resolution of ~500 Pa per stroke is achievable. c)Pressure rise after one stroke at different starting pressures in the reservoir for a reservoir volume of 1335 mL. At higher starting pressures, the pressure rise due to one stroke decreases slightly. d) Temperature rise due to pumping was less than 4 ℃ even after 30 pumping strokes. e) Pressure generated within the pump remained constant regardless of the number of applied strokes. All data points were obtained in triplicates. Error bars represent one standard deviation.

We verified the ability of our setup to achieve a range of accurate FRRs through the control of the ratio between the pressures applied on the surface of the buffer and lipids solution in the falcon tubes. To achieve this objective, we fabricated a PDMS hydrodynamic focusing microfluidic chip and tested the different FRRs we could generate inside it, Figure 4-a. A FRR as high as 47 was achievable in the hydrodynamic focusing microfluidic chip at a PR of 2.3 compared to a predicted PR of 2.1 according to equation (11). It has to be mentioned here that the FRR is typically kept within 10-15 in most microfluidic preparations of NPs (Abdelkarim et al. 2021). Although a higher FRR can produce a smaller NP size, any increase in the FRR beyond 10 results in a very low yield of the resulting NPs, requiring further concentration steps. Similarly, we were able to easily control the FRR in the commercially available herringbone micromixer chip by controlling the PR between the two bottles, Figure 4-b. A flow rate ratio of 12.5 could be achieved at a PR of 2.77.

a)

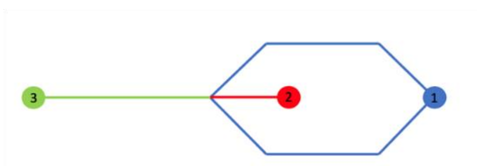

Channel dimensions	Channel 1 (Blue)	Channel 2 (Red)	Channel 3 (Green
Width (μm)	210	116	80
Height (μm)	27	30	30
Length (mm)	25	8	5
Poiseuille number ($C = Re.f$)	82.32	72.92	62.2

c)

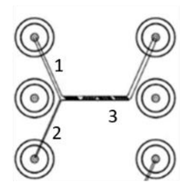

Channel dimensions	Channel 1	Channel 2	Channel 3
Width (μm)	300	300	600
Height (μm)	200	200	200
Length (mm)	8.0	8.0	9.4

b)

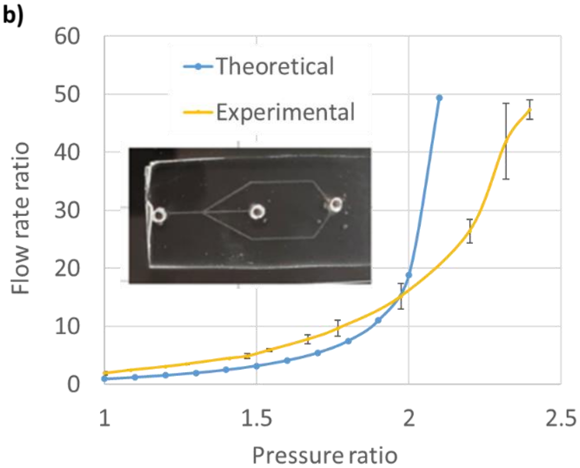

d)

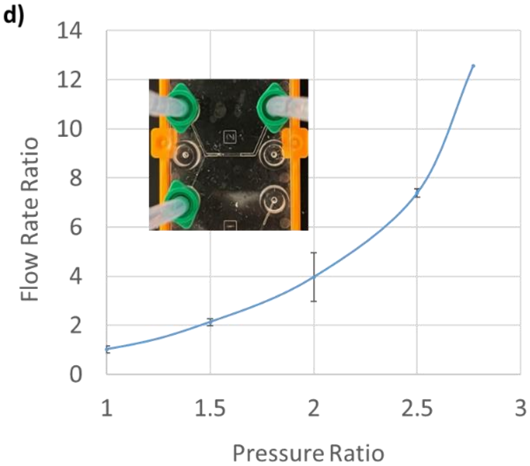

Figure 4: a) Schematic of a typical hydrodynamic flow focusing device used for preparation of nanoparticles. Port 1 is the Buffer inlet, port 2 is the lipid/polymer inlet, and port 3 is the outlet. The table below shows the dimensions of the different microchannels of the device in (a). Poiseuille number is the product of the Reynolds number times the Darcy friction factor inside a microchannel under laminar flow and is a function of the channel aspect ratio. b) The experimental and theoretical flow rate ratio vs. pressure ratio for the hydrodynamic focusing chip described in (a) and shown in the inset. c) Schematic and dimensions of the herringbone micromixer used for the preparation of liposomes. d) Experimental flow rate ratio in the herringbone micromixer chip (inset). Theoretical data were not plotted for this chip because the herringbone micromixer ridges inside the channel disturb the flow inside the channel and result in a large deviation from the theoretical calculations Error bars represent one standard deviation.

4.3 Nanoparticle Synthesis

4.3.1 Liposomes

We used the herringbone micromixer chips to synthesize liposomes at three different pressure ratios of 1.65:1, 2:1, and 2.8:1, which corresponded to FRRs of 2:1, 4:1, and 12:1. Expectedly, increasing the pressure ratio from 1.65:1 to 2.8:1 reduced the size of the liposomes by nearly threefold, from 246 nm to 79 nm, Figure 5-a. These results are on par with existing studies of NP synthesis via microfluidics, where an increase in FRR has often resulted in a decrease in the size of synthesized NPs (Agam et al. 2021, Han et al. 2021, Zhang et al. 2023). The reduction in NP diameter at higher FRRs occurs due to an increase in mass transfer and solvent exchange between the two mixing streams. The rise in pressure ratio (PR) and, consequently, the flow rate ratio (FRR) leads to an expansion of the width of the PBS stream in comparison to the width of the center lipid stream. This, in turn, accelerates the diffusion rate, leading to a quicker formation of nanoparticles with a smaller diameter (Agam et al. 2021). The polydispersity index for all three tested PR remained nearly constant at 20%, indicating an acceptable range of heterogeneity in the synthesized liposomes, Figure 5-b.

The properties of the liposomes prepared using the herringbone micromixer chip were comparable to liposomes prepared conventionally using the thin-film hydration technique, as explained in detail in a study we published recently (Agam et al. 2024). In that study, we showed that liposomes prepared using the herringbone micromixer had comparable size and stability to conventionally prepared liposomes over 4 weeks. The lipid content of the microfluidics-prepared liposomes was slightly less than that prepared conventionally. However, this did not reduce their capability of encapsulating calcein as a model drug and releasing it under the effect of ultrasound waves as an external trigger. We also demonstrated the ability to conjugate ligands to microfluidics-prepared liposomes, which increases their uptake by cells targeted specifically by the attached ligand.

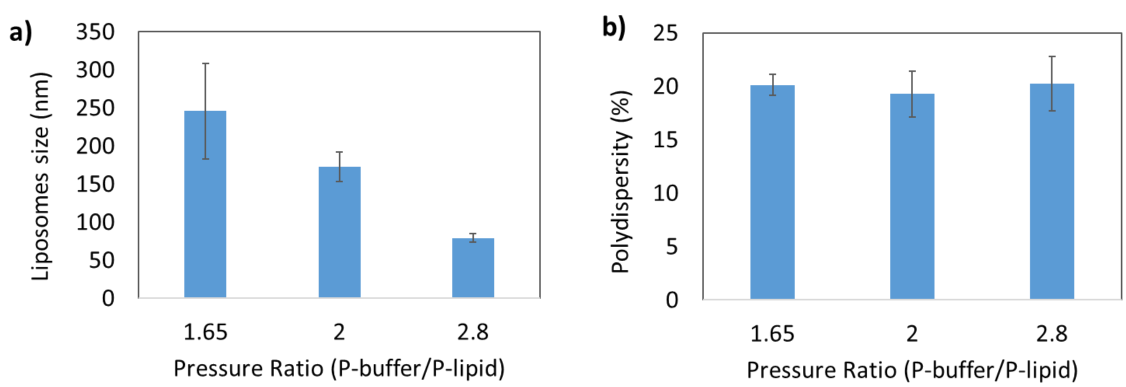

Figure 5: Characterization of the liposomes prepared inside a Herringbone micromixer using the finger-operated pumping platform. Change of a) the diameter and b) polydispersity of the resulting liposomes with pressure ratio between the two reservoir bottles. All data points were obtained in triplicates. Error bars represent one standard deviation.

4.3.2 PLGA nanoparticles

To show the versatility of our finger-operated pumping platform, we used it to prepare PLGA NPs by nanoprecipitation in the herringbone micromixer and a hydrodynamic flow-focusing device similar to the one shown in Figure 4-a. The preparation of the PLGA nanoparticles was straightforward after setting the pressure ratio between the two pumping reservoirs. Particles as small as 47 nm were obtained using the herringbone micromixer, whereas the hydrodynamic flow focusing device yielded NPs measuring 127 nm, Figure 6. The nanoparticles' polydispersity resulting from both devices was less than 20%, indicating a uniform size distribution from both devices. This data agrees with previous results of the preparation of PLGA nanoparticles by nanoprecipitation inside microchannels (Abdelkarim et al. 2021). This indicates that using our low-cost finger-operated pumping platform does not affect the nanoparticle synthesis process inside the microchannels.

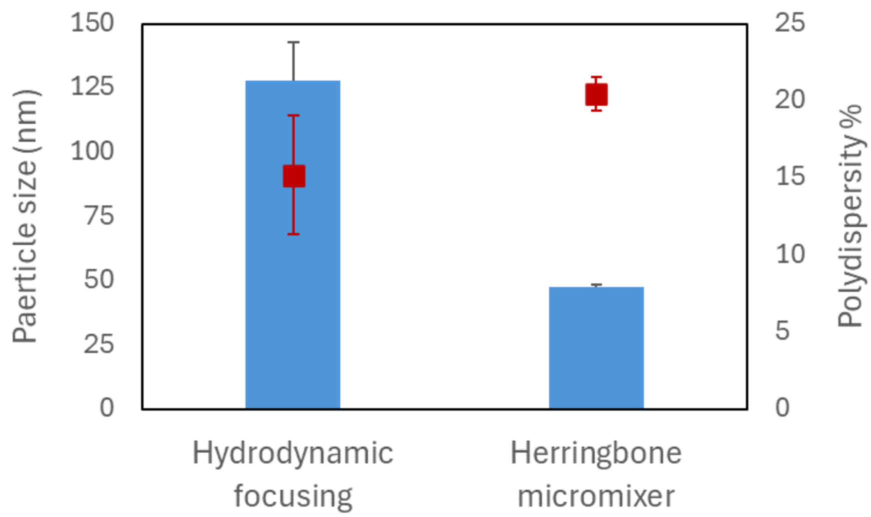

Figure 6 Preparation of PLGA nanoparticles inside a hydrodynamic flow focusing device and a herringbone micromixer using the finger-operated pumping platform. Bars indicate particle size and markers indicate polydispersity. The hydrodynamic focusing device was run at a PR of 1.2, corresponding to an FRR of 4:1 (DI water: DMF), whereas the herringbone micromixer was run at a PR=2 corresponding to a FRR=5:1 (PBS : lipids). Error bars represent one standard deviation.

5 Conclusion

The finger-operated pumping platform presented here is a very attractive solution to laboratories contemplating the use of microfluidics for nanoparticle synthesis. The platform costs only $208 without the flow sensors and is easy to assemble. Together with the availability of low-cost, off-the-shelf micromixer chips, this platform provides almost instantaneous accessibility to exploring the technology without major capital investments in microfabrication or pumping equipment. The pressure stability over relatively long durations helps avoid all the challenges resulting from the pulsating nature of the flow generated from syringe pumps. This stability facilitates NP synthesis at constant flow rates, leading to more uniform particle size and low polydispersity. Combined with the current advancements in 3D printing of microchannels, this pumping platform can potentially bring NP synthesis capabilities to almost any lab in the world.

6 References

Abdelkarim, M., N. H. Abd Ellah, M. Elsabahy, M. Abdelgawad and S. A. Abouelmagd (2021). "Microchannel geometry vs flow parameters for controlling nanoprecipitation of polymeric nanoparticles." Colloids and Surfaces A: Physicochemical and Engineering Aspects **611**: 125774.

Abualsayed, A., S. Abouelmagd and M. Abdelgawad (2019). "Miniaturized Preparation of polymeric nanoparticles using droplet manipulation on open surfaces." Micro and Nano Letters **14**(13): 1312 – 1316.

Adachi, M., S. Tsukui and K. Okuyama (2003). "Nanoparticle Formation Mechanism in CVD Reactor with Ionization of Source Vapor." Journal of Nanoparticle Research **5**(1): 31-37.

Agam, M., V. Paul, M. Abdelgawad and G. Husseini (2021). Targeted Liposomes Production in a Microfluidic Chip. 2021 IEEE 15th International Conference on Nano/Molecular Medicine & Engineering (NANOMED).

Agam, M., V. Paul, M. Abdelgawad and G. Husseini (2024). "Production of Targeted Estrone Liposomes Using a Herringbone Micromixer." IEEE Transactions on NanoBioscience: 1-1.

Andrea Cristaldi, D., A. Labanca, T. Donal Pottinger, J. Owen, E. Stulz, X. Zhang and D. Carugo (2021). "3D printed reactor-in-a-centrifuge (RIAC): Making flow-synthesis of nanoparticles pump-free and cost-effective." Chemical Engineering Journal **425**: 130656.

Aşık, M. D., M. Kaplan, B. çetin and N. Sağlam (2021). "Synthesis of iron oxide core chitosan nanoparticles in a 3D printed microfluidic device." Journal of Nanoparticle Research **23**: 62.

Bokov, D., A. Turki Jalil, S. Chupradit, W. Suksatan, M. Javed Ansari, I. H. Shewael, G. H. Valiev and E. Kianfar (2021). "Nanomaterial by Sol-Gel Method: Synthesis and Application." Advances in Materials Science and Engineering **2021**: 5102014.

Bressan, L. P., T. M. Lima, G. D. da Silveira and J. A. F. da Silva (2020). "Low-cost and simple FDM-based 3D-printed microfluidic device for the synthesis of metallic core–shell nanoparticles." SN Applied Sciences **2**(5): 984.

Chen, Z., J. Y. Han, L. Shumate, R. Fedak and D. L. DeVoe (2019). "High Throughput Nanoliposome Formation Using 3D Printed Microfluidic Flow Focusing Chips." Advanced Materials Technologies **4**(6): 1800511.

Cheng, Z., X. Yan, X. Sun, B. Shen and S. S. Gambhir (2016). "Tumor Molecular Imaging with Nanoparticles." Engineering **2**(1): 132-140.

Fink, G., F. Costamoling and R. Wille (2022). "MMFT Droplet Simulator: Efficient Simulation of Droplet-based Microfluidic Devices." Software Impacts **14**: 100440.

Gong, M. M., B. D. MacDonald, T. V. Nguyen and D. Sinton (2012). "Hand-powered microfluidics: A membrane pump with a patient-to-chip syringe interface." Biomicrofluidics **6**(4): 044102-044113.

Gujrati, M., A. Malamas, T. Shin, E. Jin, Y. Sun and Z.-R. Lu (2014). "Multifunctional Cationic Lipid-Based Nanoparticles Facilitate Endosomal Escape and Reduction-Triggered Cytosolic siRNA Release." Molecular Pharmaceutics **11**(8): 2734-2744.

Han, F. Y., W. Xu, V. Kumar, C. S. Cui, X. Li, X. Jiang, T. M. Woodruff, A. K. Whittaker and M. T. Smith (2021). "Optimisation of a Microfluidic Method for the Delivery of a Small Peptide." Pharmaceutics **13**(9).

Han, J. Y., J. N. La Fiandra and D. L. DeVoe (2022). "Microfluidic vortex focusing for high throughput synthesis of size-tunable liposomes." Nature Communications **13**(1): 6997.

Jørgensen, J. T., K. Norregaard, P. Tian, P. M. Bendix, A. Kjaer and L. B. Oddershede (2016). "Single Particle and PET-based Platform for Identifying Optimal Plasmonic Nano-Heaters for Photothermal Cancer Therapy." Scientific Reports **6**(1): 30076.

Karnik, R., F. Gu, P. Basto, C. Cannizzaro, L. Dean, W. Kyei-Manu, R. Langer and O. C. Farokhzad (2008). "Microfluidic Platform for Controlled Synthesis of Polymeric Nanoparticles." Nano Letters **8**(9): 2906-2912.

Khan, I., K. Saeed and I. Khan (2019). "Nanoparticles: Properties, applications and toxicities." Arabian Journal of Chemistry **12**(7): 908-931.

Kim, M., S. Osone, T. Kim, H. Higashi and T. Seto (2017). "Synthesis of Nanoparticles by Laser Ablation: A Review." KONA Powder and Particle Journal **34**: 80-90.

Kokalj, T., Y. Park, M. Vencelj, M. Jenko and L. P. Lee (2014). "Self-powered Imbibing Microfluidic Pump by Liquid Encapsulation: SIMPLE." Lab on a Chip **14**(22): 4329-4333.

Kumar, P. S., S. Madapusi and S. Goel (2023). "Sub-second synthesis of silver nanoparticles in 3D printed monolithic multilayered microfluidic chip: Enhanced chemiluminescence sensing predictions via machine learning algorithms." International Journal of Biological Macromolecules **245**: 125502.

Lee, S., H. Kim, W. Lee and J. Kim (2018). "Finger-triggered portable PDMS suction cup for equipment-free microfluidic pumping." Micro and Nano Systems Letters **6**(1): 1.

Li, X. and C. O. Chui (2018). "Engineering finger-operated peristaltic pumps." Microfluidics and Nanofluidics **22**(1): 14.

Liu, D., C. Li, F. Zhou, T. Zhang, H. Zhang, X. Li, G. Duan, W. Cai and Y. Li (2015). "Rapid synthesis of monodisperse Au nanospheres through a laser irradiation-induced shape conversion, self-assembly and their electromagnetic coupling SERS enhancement." Scientific reports **5**(1): 7686.

Liu, Y. and X. Jiang (2017). "Why microfluidics? Merits and trends in chemical synthesis." Lab on a Chip **17**(23): 3960-3978.

Michelon, M., D. R. B. Oliveira, G. de Figueiredo Furtado, L. Gaziola de la Torre and R. L. Cunha (2017). "High-throughput continuous production of liposomes using hydrodynamic flow-focusing microfluidic devices." Colloids and Surfaces B: Biointerfaces **156**: 349-357.

Moscovici, M., W.-Y. Chien, M. Abdelgawad and Y. Sun (2010). "Electrical power free, low dead volume, pressure-driven pumping for microfluidic applications." Biomicrofluidics **4**(4): 046501.

Murthy, S. K. (2007). "Nanoparticles in modern medicine: state of the art and future challenges." Int J Nanomedicine **2**(2): 129-141.

Ngoy, J. M., N. Wagner, L. Riboldi and O. Bolland (2014). "A CO2 Capture Technology Using Multi-walled Carbon Nanotubes with Polyaspartamide Surfactant." Energy Procedia **63**: 2230-2248.

Nguyen, M. T., H. Zhang, L. Deng, T. Tokunaga and T. Yonezawa (2017). "Au/Cu Bimetallic Nanoparticles via Double-Target Sputtering onto a Liquid Polymer." Langmuir **33**(43): 12389-12397.

Niculescu, A.-G., C. Chircov, A. C. Bîrcă and A. M. Grumezescu (2021) "Nanomaterials Synthesis through Microfluidic Methods: An Updated Overview." Nanomaterials **11** DOI: 10.3390/nano11040864.

Park, J. and J.-K. Park (2019). "Integrated microfluidic pumps and valves operated by finger actuation." Lab on a Chip **19**(18): 2973-2977.

Petcharoen, K. and A. Sirivat (2012). "Synthesis and characterization of magnetite nanoparticles via the chemical co-precipitation method." Materials Science and Engineering: B **177**(5): 421-427.

Salkho, N. M., V. Paul, P. Kawak, R. F. Vitor, A. M. Martins, M. Al Sayah and G. A. Husseini (2018). "Ultrasonically controlled estrone-modified liposomes for estrogen-positive breast cancer therapy." Artificial Cells, Nanomedicine and Biotechnology **46**(sup2): 462-472.

Sanka, R., J. Lippai, D. Samarasekera, S. Nemsick and D. Densmore (2019). "3DμF - Interactive Design Environment for Continuous Flow Microfluidic Devices." Scientific Reports **9**(1): 9166.

Shaalan, N. M., T. Yamazaki and T. Kikuta (2011). "Influence of morphology and structure geometry on NO2 gas-sensing characteristics of SnO2 nanostructures synthesized via a thermal evaporation method." Sensors and Actuators B: Chemical **153**(1): 11-16.

Shawky, S. M., D. Bald and H. M. E. Azzazy (2010). "Direct detection of unamplified hepatitis C virus RNA using unmodified gold nanoparticles." Clinical Biochemistry **43**(13-14): 1163-1168.

Sweet, E., R. Mehta, Y. Xu, R. Jew, R. Lin and L. Lin (2020). "Finger-powered fluidic actuation and mixing via MultiJet 3D printing." Lab on a Chip **20**(18): 3375-3385.

Thurgood, P., S. A. Suarez, S. Chen, C. Gilliam, E. Pirogova, A. R. Jex, S. Baratchi and K. Khoshmanesh (2019). "Self-sufficient, low-cost microfluidic pumps utilising reinforced balloons." Lab on a Chip **19**(17): 2885-2896.

Thurgood, P., J. Y. Zhu, N. Nguyen, S. Nahavandi, A. R. Jex, E. Pirogova, S. Baratchi and K. Khoshmanesh (2018). "A self-sufficient pressure pump using latex balloons for microfluidic applications." Lab on a Chip **18**(18): 2730-2740.

Zhang, H., J. Yang, R. Sun, S. Han, Z. Yang and L. Teng (2023). "Microfluidics for nano-drug delivery systems: from fundamentals to industrialization." Acta Pharmaceutica Sinica B.

Zhang, L., Q. Chen, Y. Ma and J. Sun (2020). "Microfluidic Methods for Fabrication and Engineering of Nanoparticle Drug Delivery Systems." ACS Applied Bio Materials **3**(1): 107-120.